Interactions of Aryloxyphenoxypropionic Acids with Sensitive and Resistant Acetyl-Coenzyme A Carboxylase by Homology Modeling and Molecular Dynamic Simulations

Xiao-Lei Zhu, Li Zhang, Qiong Chen, Jian Wan, and Guang-Fu Yang*

Key Laboratory of Pesticide & Chemical Biology of Ministry of Education, College of Chemistry, Central China Normal University, Wuhan 430079, People's Republic of China

Received January 25, 2006

Acetyl-coenzyme A carboxylase (ACCase) has been identified as one of the most important targets of herbicides. In the present study, we constructed homology models of the carboxyl-transferase (CT) domain of ACCase from sensitive and resistant foxtail and used these models as templates to study the molecular mechanism of herbicide resistance and stereochemistry−activity relationships of aryloxyphenoxypropionates (APPs). In the homology modeling structures, the dimer of the CT domain was formed by the side-to-side arrangement of the two monomers, in such a way that the N domain of one molecule is placed next to the C domain of the other. The dimeric association of sensitive foxtail CT was found to differ from that of resistant foxtail CT, and the spatial orientation of two key residues, Leu-695 and Ile-695, in these dimers also differed. The mutation of Ile to Leu may perturb the conformation of the dimeric interface, which may account for the molecular mechanism of herbicide resistance. Further docking analysis indicated that the binding model of high-active compounds is similar to that in the crystal structure of the enzyme−ligand complex. The different spatial orientations of ester groups of the isomers of APPs may explain the stereochemistry−activity relationship. Ser-698 formed a H-bonding interaction with all of the docked ligands, while Tyr-728 formed a $\pi-\pi$ stacking interaction with some of the APPs. These findings may enhance our understanding of the molecular mechanism of herbicide resistance and stereochemistry−activity relationships, which may provide a new starting point for the identification of more potent inhibitors against both sensitive and resistant ACCase.

INTRODUCTION

Acetyl-coenzyme A carboxylase (ACCase; EC 6.4.1.2) is a key enzyme in fatty acid biosynthesis in both eukaryotes and prokaryotes.[1−3] ACCase is a biotinylated enzyme that catalyzes the carboxylation of acetyl-CoA to produce malonyl-CoA.[4] This reaction is a two-step process, in which the first step consists of the ATP-dependent carboxylation of the biotin group on the carboxyl carrier domain by the biotin-carboxylase activity, and the second step consists of the transfer of the carboxyl group from biotin to acetyl-CoA by the carboxyl-transferase (CT) activity. In plants, two ACCase isoforms have been identified, one in the cytosol and the other in the chloroplast.[5,6] In all plants studied to date, the cytosolic ACCase is a multidomain enzyme, which provides malonyl-CoA for the synthesis of very long chain fatty acids and flavonoids and for malonylation. The chloroplastic ACCase isoform catalyzes the first committed step in fatty acid biosynthesis. In most plant species, chloroplastic ACCase is a multisubunit enzyme. However, in *Poaceae* (grasses), the chloroplastic ACCase is a multidomain enzyme encoded by a nuclear gene distinct from that coding for the cytosolic ACCase isoform.[7]

The chloroplastic, multidomain form of ACCase has been identified as the target of two chemically distinct classes of herbicides: aryloxyphenoxypropionates (APPs) and cyclohexanediones (CHDs).[1,8−9] Both of these classes of herbicides are linear, noncompetitive inhibitors of various ACCase substrates.[10,11] The activity of CT is inhibited by these herbicides, thus blocking the transfer of the carboxyl group to acetyl-CoA. Multisubunit-type ACCases are insensitive to CHDs and APPs, whereas cytosolic, multidomain-type ACCases are significantly less sensitive to CHDs and APPs than chloroplastic, multidomain-type ACCases. Thus, most plant species other than *Poaceae* are insensitive to these herbicides, as are most other eukaryotes and prokaryotes, making APPs and CHDs effective graminicides.

APPs and CHDs are thought to share overlapped binding sites on ACCase and to compete with malonyl CoA for binding at these sites.[1,12] The frequent use of APPs and CHDs has resulted in many grass weed species developing resistance to these herbicides.[13−18] In most cases, resistance is due to mutation of the target enzyme, ACCase, making it less sensitive to inhibition by these herbicides. However, the molecular mechanism surrounding the binding of APPs and CHDs to ACCase is not clear. One major obstacle to elucidating the molecular mechanism is a lack of the corresponding three-dimensional (3D) structure of ACCase from plants.

Recently, the crystal structures of the CT domain (PDB codes 1OD2 and 1OD4) of yeast (*Sacharomyces cerevisiae*) ACCase and its complex with APPs (PDB codes 1UYR and

* Corresponding author phone: 86-27-6786-7706; fax: 86-27-6786-2022; e-mail: gfyang@mail.ccnu.edu.cn.

10.1021/ci0600307 CCC: $33.50
Published on Web 05/16/2006

Table 1. Sequence Identity between the Selected Templates and Foxtail Enzymes

identity (%)	1OD2B[a]	1OD2A[a]	1W2XC[a]	1UYTB[a]	1UYTC[a]	1OD4A[a]
foxtail-S	51.73	51.73	52.32	52.32	52.32	/ [b]
foxtail-R	51.83	51.83	52.44	52.44	/ [b]	52.44

[a] Capital letter means one subunit of the protein was used. [b] This template was not used.

1UYS) were determined at 2.7 and 2.5 Å resolution,[11,19] respectively, providing a starting point for the study of ligand−receptor interactions and the rational design of inhibitors of these enzymes. In seeking to develop novel herbicides that inhibit both sensitive and resistant forms of ACCase in grass weeds, we have created theoretical models of the three-dimensional dimeric structures of CT from sensitive and resistant foxtail millet (*Setaria italica*) by using homology modeling and subsequent molecular dynamic simulation procedures. Subsequently, we analyzed the ligand−receptor interactions by docking a series of herbicidal APPs into the binding site of these proposed three-dimensional dimeric structures. These models revealed a molecular explanation for herbicidal resistance, as well as the stereochemistry−activity relationships. We believe that these results can be considered a new starting point for a more extensive understanding of the resistance mechanism linked to this target at the molecular level.

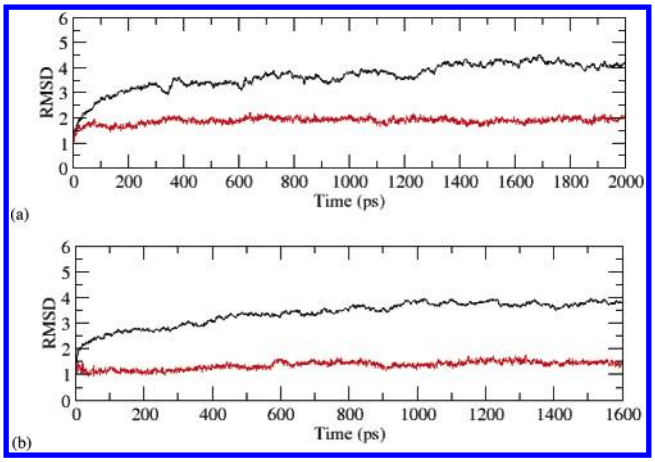

Figure 1. Plots of the RMSDs of foxtail-2S (a) and foxtail-2R (b). The black line represents the RMSD of backbone atoms, and the red line represents the RMSD of the conserved residues.

MATERIALS AND METHODS

Sequence Alignment. The amino acid sequences of both forms of *S. italica* ACCase (sensitive foxtail millet, AY219174, i.e., foxtail-S; resistant foxtail millet, AY219175, i.e., foxtail-R) have been reported[20] and can be obtained from the NCBI Web site.[21] Amino residues 1638−2191 in these two sequences were renumbered 1−553. The alignment of the sequence of foxtail-S and foxtail-R with one chain of the dimer of the yeast CT domain was performed by means of the CLUSTALW package (http://www.ebi.ac.uk /clustalw) with the default parameters (see the Supporting Information).

Model Building. The sequences of foxtail-S and foxtail-R were submitted to the SWISS-MODEL sever (Automated Comparative Protein Modeling Sever, version 3.5, Glaxo-Wellcome Experiment Research, Geneva, Switzerland) [22] for comparative structural modeling. Structures having more than 25% sequence identity with the target sequence in ExPDB (extracted from the PDB database) were selected as templates for homology modeling. The sequences were structurally aligned to identify the structural conserved region, and several suitable templates were selected. Table 1 shows the sequence identity between the selected templates (PDB code: 1OD2,[11] 1OD4,[11] 1UYT,[19] 1UYS,[19] and 1W2X[23]) and the sequences of the foxtail enzymes. PROCHECK[24,25] was used to check the stereochemical quality of these two homology models. All hydrogen atoms were generated to fill the unoccupied valence of heavy atoms at the neutral state in Insight II (2000).

Dynamic Simulations. Because the crystal structure of the CT domain from yeast is a dimer, the homology dimeric structure of foxtail should be obtained first. Two monomeric chains were superimposed onto the crystal structure of the CT domain from yeast (1OD2), to keep the same relative orientation of the two subunits. The dimers of sensitive (foxtail-2S) and resistant (foxtail-2R) foxtail were obtained using the Merge module in Sybyl 7.0. To obtain stable conformations and reduce steric clashes, these two dimers were subjected to further molecular dynamic (MD) simulation using the SANDER module of the AMBER 7 package.[26] Both systems were neutralized by adding Na^+ and then solvated in an octahedral box of TIP3P water molecules, [27] which extended at least 6 and 5 Å from any given protein atom for foxtail-2S and foxtail-2R, respectively. The system setup for simulations included the particle mesh Ewald method [28] for the long-range electrostatics, a 10 Å cutoff for nonbonding van der Waals interactions, and periodic boundary conditions. All bonds involving hydrogen atoms were constrained using the SHAKE algorithm.[29] Constant temperature and pressure (300 K/1 atm) were maintained using the Berendsen coupling algorithm [30] with a time constant for heat bath coupling of 2 ps. A time step of 1 fs was used to integrate the equations of motion.

Before starting the production-run phase, the following equilibration protocol was applied to both systems. First, the systems were minimized for 1500 steps SD and 1500 steps CG, followed by the minimization of water for 3000 steps while holding the protein frozen. Finally, the two systems were slowly heated from 10 to 300 K over 100 ps before MD simulation for 2000 ps (foxtail-2S) or 1600 ps (foxtail-2R). Coordinates were saved every 1 ps during the entire simulation process. The root-mean-square deviations (RMSD) of the backbones and the conserved residues of the two proteins over the simulation time were derived using the PTRAJ module as shown in Figure 1. The averaged structures of foxtail-2S and foxtail-2R were extracted from 1400 to 2000 ps and from 1000 to 1600 ps, respectively, and subjected to a subsequent minimization with a RMS gradient of 0.05 kcal/(mol Å) with a Tripos force field in Sybyl 7.0. The obtained models were checked by PROCHECK for stereochemical quality and by PROSA2003 [31] for the energy of each residue.

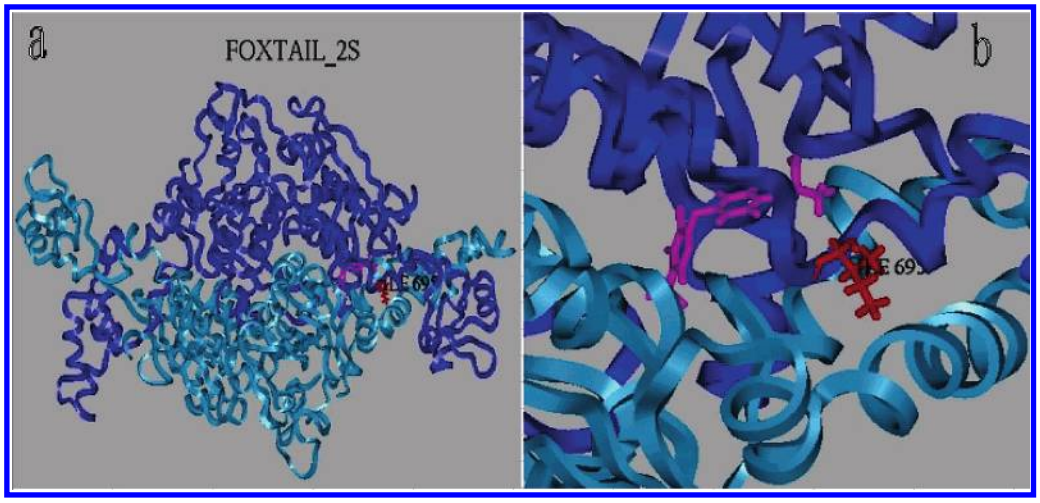

Figure 2. (a) Ribbon structure of the foxtail-2S dimer, in which the monomers are shown in blue and light blue. (b) Close up of the area around the residue Ile-695 shown as a red stick. To ease reading of the spatial position around residue Ile-695, a ligand was placed into the active site, represented by a magenta stick.

Molecular Docking. To understand the molecular mechanism of the interaction of APPs with ACCase, molecular docking was carried out using the advanced docking Affinity/Insight II program (MSI, San Diego, CA, 2000). On the basis of the crystal structure of yeast CT, [11] the active site is located at the interface of the dimer. Ligands **1**∼**5**, which were built using Builder/Insight II and optimized with the default parameters, were docked into the active site of foxtail-2S employing the CVFF force field. The starting orientations of ligands **1**∼**5** were determined in such a way that the intermolecular interaction energies were reduced to reasonable levels with manual adjustments after the ligands were placed in the pocket. In the process of docking, residues within 5 Å of the ligand were defined as the binding subset, while the backbone of the protein defined as the atoms not in the binding subset was held rigid. First, 30 distinct docking poses, created by random translation or rotation of the ligand followed by a 100 steps of minimization, were collected using the Monte Carlo minimization method. Only those docking models were retained in which the ligands differed by a minimum RMS distance of 1 Å (RMS tolerance) and had an energy range within 100 kcal of that of the lowest energy structure. During this stage, the Quartic_vdw_no_Coul method was used to calculate nonbonding energy. This method employs a purely repulsive bounded quartic potential for modeling van der Waals interactions, and the Coulombic interactions are zero, in which the scale of van der Waals interactions was set to 0.1. In the subsequent stage, combined with the simulated annealing procedure, a more refined cell-multipole method was applied to the calculation of nonbonding interactions. In this stage, the scales of van der Waals interactions, Coulombic interactions, and H-bond interactions were all set to 0.1. The final model was selected on the basis of the results of Ludi_score (Energy_Estimate_3) and the nonbonding energy.

RESULTS AND DISCUSSION

Homology Modeling and Molecular Dynamic Simulations. Although foxtail-S and foxtail-R have the same number of amino acid residues, they differ at residues 142 and 485, which are Ile and Gly, respectively, for foxtail-S, and Leu and Glu, respectively, for foxtail-R. We ignored the effect of residue 485 in the following studies because this residue lies at the end of the monomer and will not contribute to the binding energy. In contrast, residue 142, which corresponds to residue 695 in the dimer, may play a key role in the binding of herbicides to the enzyme because it is located in the cavity of the dimer. Ile-142 in sensitive graminases has been shown to be mutated to other residues in dicots and nongraminaceous monocots, which are resistant to herbicidal APPs and CHDs.[32−34]

There is over 51% sequence identity between the CT domains of yeast ACCase and foxtail millet ACCase. Therefore, structure information on the crystal of the yeast CT domain should be applicable to the 3D homology modeling of the foxtail millet CT domain. In addition, the results of Délye and Michel[35] indicated that ACCases from several grasses had higher sequence identities, which are about 91.5% in plastidic and about 77.1% between plastidic and cytosolic. So, the 3D structure of the CT domain in foxtail could be regarded as the model structure of the CT domain in plants.

The stereochemical quality of the models obtained from homology modeling and molecular dynamic simulations were checked with the PROCHECK program (see the Supporting Information). The majority of the residues of the two models were found to occupy the most favored regions of Ramachandran plots, and the other residues occupied the additional allowed regions. In foxtail-2S, 75.3% of the residues were presented in the most favored regions, 23.2% in the additional regions, 1.3% in the generously allowed regions, and only 0.2% in the disallowed regions. For foxtail-2R, 79.0%, 19.7%, 0.9%, and 0.4% of the residues were presented in these four regions, respectively. These figures and further assessment results with the Prosa2003 program for the interaction energy of each residue (also see the Supporting Information) indicated that these homology models were reasonable and reliable.

The results of X-ray diffraction indicated that the active site of the enzyme is located at the interface of the dimer, with approximately equal contributions from the N and C domains of the two monomers.[11] As shown in Figures 2 and 3, the homology-modeled dimer of the CT domain is formed

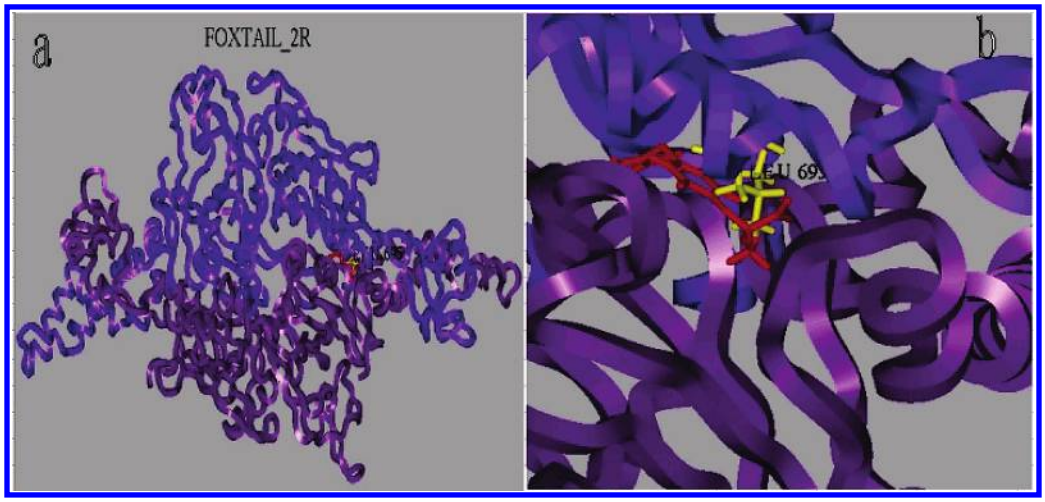

Figure 3. (a) Ribbon structure of the foxtail-2R dimer, in which the monomers are shown in purple and dark purple. (b) Close up of the area around residue Leu-695 shown as a yellow stick. To ease reading of the spatial position around residue Leu-695, a ligand was placed into the active site, represented by a red stick.

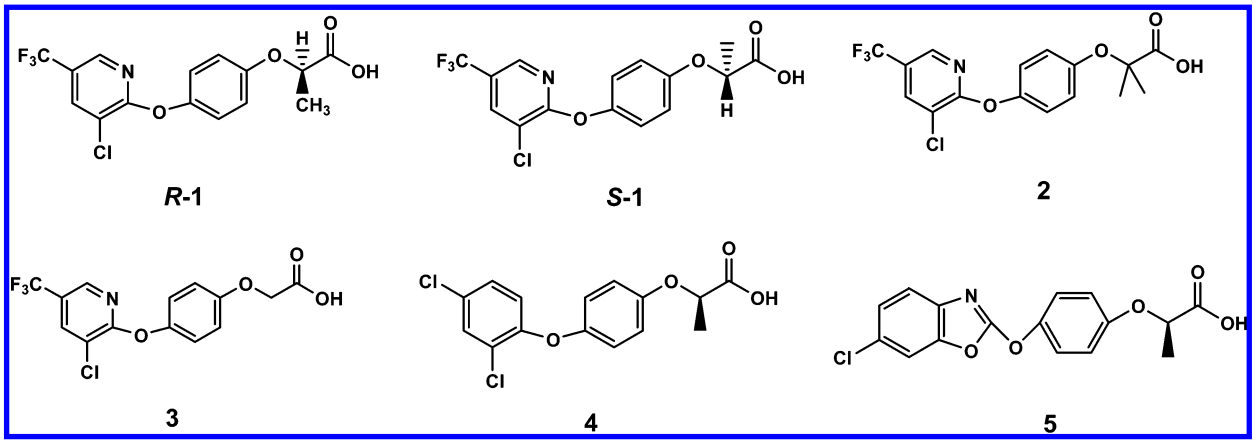

Figure 4. Ligands used in docking analyses.

by the side-to-side arrangement of the two monomers, in such a way that the N domain of one molecule is placed next to the C domain of the other. Through visual inspection, the dimeric association of foxtail-S CT was different from that of foxtail-R CT. Leu-1705 in the crystal structure of yeast CT was found to allele to Leu-695 in foxtail-R CT and Ile-695 in foxtail-S CT. The side-chain conformations of Leu-695 in foxtail-R CT and Ile-695 in foxtail-S CT were similar in the monomeric states of CT, but the spatial orientation of residue-695 in the dimers differed upon dimer formation. In foxtail-2S, Ile-695 extended its side chain outside the active site, while Leu-695 in foxtail-2R extended its side chain toward the cavity of the active site, inhibiting the entrance of ligand. The different orientations of Leu-695 and Ile-695 may provide a molecular explanation for the mechanism of herbicidal resistance.

Subsequently, the hydrogen bonds presented at the dimer interface and the solvent-accessible surface were analyzed using the Measure and Solvation modules in Insight II, respectively. The hydrogen-bond pattern of Ile-695 in these two models appears to be different. In foxtail-2S, this residue formed hydrogen bonds with residue Asn-458, while Ile-695 in foxtail-2R did not form any hydrogen bonds with other residues. In addition, the number of hydrogen bonds decreases from 43 in foxtail-2S to 30 in foxtail-2R (see the Supporting Information). These results supported the hypothesis that the mutation of Ile to Leu perturbed the dimeric interface and then reduced the binding energy of the herbicides.[36] In addition, the solvent-accessible surface areas of foxtail-2S and foxtail-2R are about 50297 and 45516 Å^2, respectively, indicating that the two monomers of foxtail-S combined more loosely than those of foxtail-R, making the binding sites in foxtail-2S more accessible.

Therefore, our results showed that the mutation of Ile to Leu at position 695 directly not only perturbs the conformation of the dimeric interface but also interferes with the correct enzymatic activity. Our results indicated that an analysis of a complete 3D structure model could deepen the understanding of the impact and unexpected effects of point mutation at a global level far from the mutation itself.[37]

Molecular Docking. Because of the symmetry of the CT dimer, only one of the two active sites in the models was considered in the procedure of molecular docking. Under physiological conditions, esters of APPs can transform readily via hydrolysis into the corresponding carboxylic acids, which are the active forms of APPs.[38,39]At the same time, a carboxyl form was observed in the crystal structure of the CT domain of yeast ACCase in complex with haloxyfop, an herbicidal APP.[19] Therefore, the carboxyl form of APPs, whose structures were shown in Figure 4, was used in our docking analyses. The IC_{50} value of the racemate of compound **1** is 0.9 μM, while that of the R isomer is 0.5,

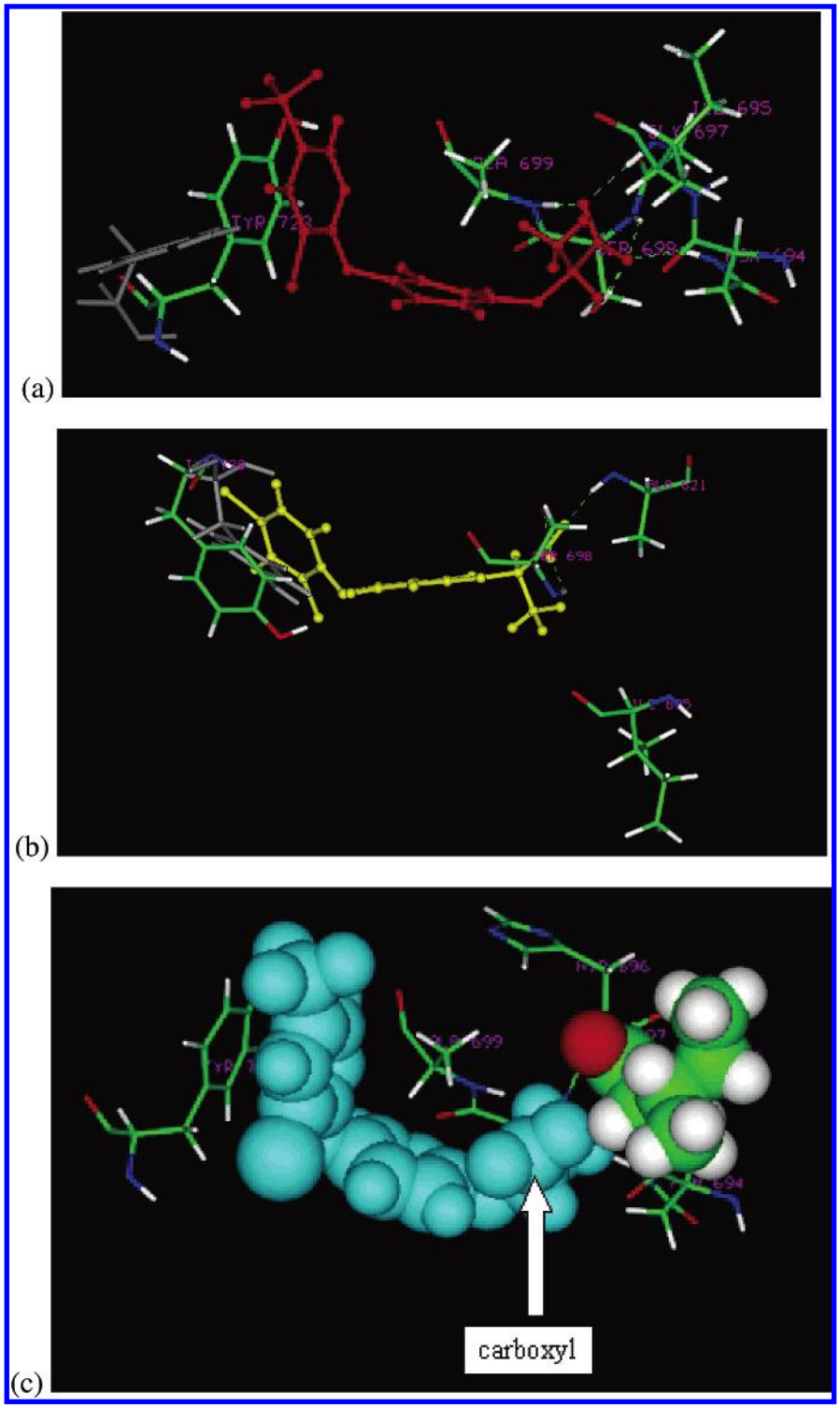

Figure 5. (a) Binding model of compound ***R*-1** (red) in the active site represented as a stick model. (b) Binding model of compound **4** (yellow) in the active site represented as a stick model. (c) Close up of the clash between compound ***S*-1** (cyan) and residue Ile-695. To visually determine the conformational change of the active site, only important residues that experience big conformational changes are shown. Gray represents the conformation before docking, while the conformation after docking is shown in Insight II system color. The green dotted lines indicate hydrogen bonds. The conformation of ***S*-1** was obtained by converting the ester group of the corresponding docking conformation of compound ***R*-1**.

almost half of that of its racemate. So a half value of the IC_{50} of the corresponding racemate was applied for compounds **4** and **5** in the following docking analyses.

The docking results of compounds ***R*-1** and **4** show that the binding models of these compounds are similar to those found from the crystal structures of yeast CT (Figure 5a,b). The conformation of the active site in foxtail-2S was changed after the ligands were docked. Most importantly, the side chain of Tyr-728 was found to cover the hydrophobic core of the dimer interface in the free enzyme [22] and to assume a new position in the docking complex, forming a $\pi-\pi$ stacking interaction with the pyridyl ring of compound ***R*-1** and the phenyl ring of compound **4**. Meanwhile, residues 694−699 became disordered in the docking complex and

Table 2. ACCase Activities[40,41] and Docking Results

compd	IC_{50} μM (maize)	Ludi score	$\pi-\pi$ stacking site	H-bonding site
***R*-1**	0.5	688	Tyr-728	Asn-694, Gly-697, Ala-699, Ser-698
***S*-1**	>100	448		
2	3.7	547	Tyr-728	Ile-725, Ala-621, Ser-698
3	8.8	656		Gly-697, Ser-698, Ala-699
4	0.75	632	Tyr-728	Ala-621, Ser-698
5	0.5	690	Tyr-728	Ile-725, Ser-698

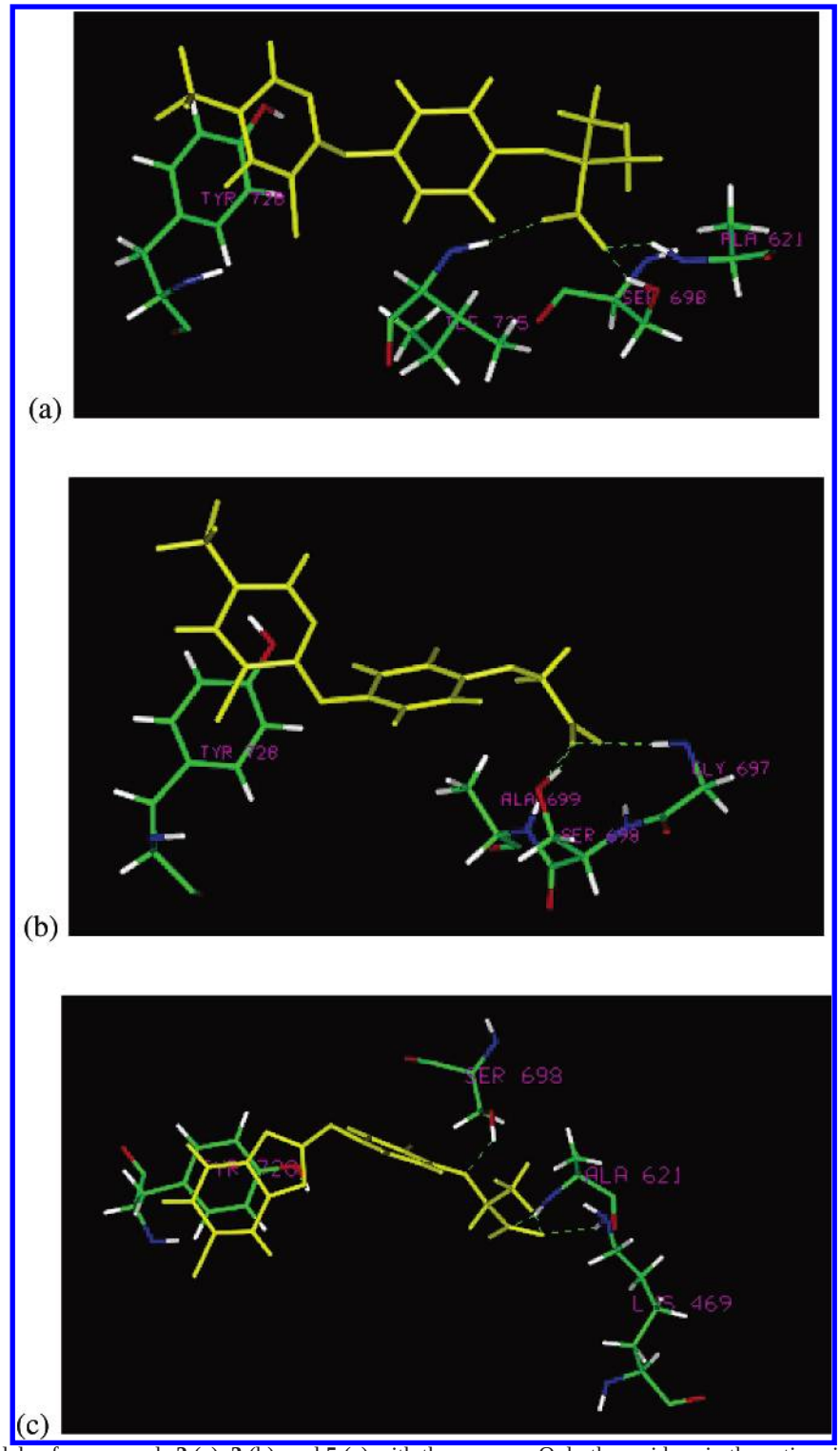

Figure 6. Binding models of compounds **2** (a), **3** (b), and **5** (c) with the enzyme. Only the residues in the active site were shown as a stick model. To visually determine the conformational change at the active site, only important residues that experience big conformational changes are shown. The green dotted lines indicate hydrogen bonds.

interacted with the ligand via steric and electrostatic interactions. In addition, an H-bonding analysis indicated that residues Asn-694, Gly-697, Ser-698, and Ala-699 form hydrogen bonds with compound ***R*-1**, while residues Ala-

621 and Ser-698 form hydrogen bonds with compound **4**. Ala-621 is homologous to residue Ala-1627 of subunit A in 1UYR, which also forms hydrogen bonds with the inhibitor. These results further confirm the reliability of these homology models and that the selection criteria for the binding model of these docking compounds were reasonable.

After compound ***R*-1** was bounded to the active site, the geometrical center of Tyr-728 was found to translate to 3.0 Å, while the side chain of this residue rotated by ~120° to avoid clashing with the ligand, and the geometrical center of the active site translated to 0.47 Å (Figure 5a). Similar changes were also observed for compound **4** (Figure 5b), in that the geometrical centers of Tyr-728 and the active site translated to 1.0 and 0.25 Å, respectively, and the side chain of Tyr-728 rotated by ~50°. The orientation of the carboxyl of compounds ***R*-1** and **4** was opposite that of Ile-695 (Figure 5a,b). If the compound **1** takes the S conformation, the carboxyl will clash with Ile-695 (Figures 5c), resulting in a decrease of binding energy, which was confirmed by the results of Ludi_Score (Table 2; compound ***S*-1** with IC_{50} > 100 μM had the lowest Ludi_Score).

The binding models of compound **2**, **3**, and **5** were shown in Figure 6. These docking results indicated that residue Ser-698 always formed a hydrogen bond with the docked ligands. At the same time, a $\pi-\pi$ stacking interaction between the phenyl of residue Tyr-728 and the aryl groups of some APPs was also observed. In addition, from the docking results, we also found that the orientation of the carboxyl group in these compounds was different (data not shown). If we selected residue Ile-695 as a reference, the carboxyl groups of all of the docked compounds took an almost opposite orientation to Ile-695. The above results revealed that each compound might bind with the target enzyme in a unique way.

CONCLUSION

In summary, we constructed three-dimensional structures of the CT domain of foxtail-S and foxtail-R by homology modeling and molecular dynamic simulations, whose reliabilities were confirmed using the PROCHECK and Prosa2003 programs. In the homology modeling structures, the dimer of the CT domain was formed by the side-to-side arrangement of the two monomers, in such a way that the N domain of one monomer is placed next to the C domain of the other. The dimeric association of foxtail-S CT was found to differ from that of foxtail-R, and the Ile to Leu mutation may perturb the conformation of the dimeric interface. The side-chain conformations of Leu-695 in foxtail-R CT and Ile-695 in foxtail-S CT were similar in the monomeric states of CT, but the spatial orientation of residue 695 in the dimers differed upon dimer formation. Further docking analysis indicated that the binding model of highly active compounds was similar to that in the crystal structure of enzyme−ligand complexes. Ser-698 forms a H bond with all of the docked ligands. Tyr-728 interacted with some high-active APPs via $\pi-\pi$ stacking. These results indicated that residues Ser-698 and Tyr-728 may play an important role in the binding of CT to herbicides. We believe that the present study will help clarify the molecular mechanism of herbicidal resistance and stereochemistry−activity relationships, which will provide a new starting point for the discovery of more potent inhibitors of sensitive and resistant ACCase.

ACKNOWLEDGMENT

The present work was supported by the National "973" Project (2003CB114400), National Natural Science Foundation of China (numbers 20572030, 20432010, and 20476036), Key project of Ministry of Education (numbers 103116 and 104205), Program for New Century Excellent Talents at the University of China, and Program for Excellent Research Group of Hubei Province (number 2004ABC002).

Supporting Information Available: The multiple sequence alignment, Ramachandran plots and Prosa2003 test result, and the H-bond analysis of the two foxtail-2S and foxtail-2R monomers. This material is available free of charge via the Internet at http://pubs.acs.org.

REFERENCES AND NOTES

(1) Burton, J. D.; Gronwald, J. W.; Keith, R. A.; Somers, D. A.; Gengenbach, B. G.; Wyse, D. L. Kinetics of inhibition of acetyl-coenzyme A carboxylase by sethoxydim and haloxyfop. *Pestic. Biochem. Physiol*. **1991**, *39*, 100−109.
(2) Rendina, A. R.; Felts, J. M. Cyclohexandione herbicides are selective and potent inhibitors of acetyl-CoA carboxylase from grasses. *Plant Physiol*. **1988**, *86*, 983−986.
(3) Egli, M. A.; Gengenbach, B. G.; Gronwald, J. W.; Somers, D. A.; Wyse, D. L. Characterization of maize acetyl-coenzyme A carboxylase. *Plant Physiol*. **1993**, *101*, 499−506.
(4) Nikolau, B. J.; Ohlrogge, J. B.; Wurtel, E. S. Plant biotin-containing carboxylase. *Arch. Biochem. Biophys*. **2003**, *414*, 211−222.
(5) Sasaki, Y.; Konishi, T.; Nagano, Y. The compartmentation of acetyl-coenzyme A carboxylase in plants. *Plant Physiol*. **1995**, *108*, 445−449.
(6) Post-Beittenmiller, D. Biochemistry and molecular biology of wax production in plants. *Annu. Rev. Plant Physiol. Plant Mol. Biol*. **1996**, *47*, 405−430.
(7) Konishi, T.; Shinohara, K.; Yamada, K.; Sasaki, Y. Acetyl-CoA carboxylase in higher plants: Most plants other than gramineae have both the prokaryotic and eukaryotic forms of this enzyme. *Plant Cell. Physiol*. **1996**, *37*, 117−122.
(8) Steve, R. W.; Christopher Hall, J. Monoclonal-based elisa for the identification of herbicidal cyclohexanedione analogues that inhibit graminaceous acetyl coenzyme-A carboxylase. *J. Agric. Food Chem*. **2000**, *48*, 1210−1218.
(9) Hernánde, M.; Río, A.; Esteve, T.; Prat, S.; Pla, M. A rapeseed-specific gene, Acetyl-CoA carboxylase, can be used as a reference for qualitative and real-time quantitative PCR detection of transgenes from mixed food samples. *J. Agric. Food Chem*. **2001**, *49*, 3622−3627.
(10) Rendina, A. R.; Craig-Kennard, A. C.; Beaudion, J. D.; Breen, M. K. Inhibition of acetyl coenzyme-A carboxylase by two classes of grass-selective herbicides. *J. Agric. Food Chem*. **1990**, *38*, 1282−1287.
(11) Zhang, H.; Yang, Z. R.; Shen, Y.; Tong, L. Crystal structure of the carboxylase domain of acetyl coenzyme-A carboxylase. *Science* **2003**, *299*, 2064−2067.
(12) Rendina, A. R.; Campopiano, O.; Marsili, E.; Hixon, M.; Chi, H.; Taylor, W. S.; Hagenah, J. A. Overlap between herbicidal inhibitors of acetyl coenzyme-A carboxylase: Enhanced binding of cyclic triketones, a novel triketones, a novel class of graminicide. *Pestic. Sci*. **1995**, *43*, 368−371.
(13) Nick, M.; Stephen, B. P.; Christopher, P. Mechanisms of resistance to acetyl-coenzyme A carboxylase-inhibiting herbicides in a *Hordeum ieporinum* population. *Pest Manage. Sci*. **2000**, *56*, 441−447.
(14) Kay, M. C.; David, S. N.; Julian, O. C.; Stephen, R. M. Resistance to ACCase-inhibiting herbicides and isoproturon in UK populations of *Lolium multiflorum*: Mechanisms of resistance and implications for control. *Pest Manage. Sci.* **2001**, *57*, 587−597.
(15) Stephen, R. M.; Kay, M. C.; Amanda, C. B.; Linda, H.; Linda, M. F. Characterisation of target-site resistance to ACCase-inhibiting herbicides in the weed *Alopecurus myosuroides* (black-grass). *Pest Manage. Sci*. **2003**, *59*, 190−201.
(16) Volenberg, D.; Stoltenberg, D. Altered acetyl-coenzyme A carboxylase confers resistance to clethodim, fluazifop and sethoxydim in *Setaria faberi* and *Digitaria sanguinalis*. *Weed Res*. **2002**, *42*, 342−350.
(17) Incledon, B. J.; Christopher Hall, J. Inhibition of ACCase220 and ACCase240 isozymes from sethoxydim-resistant and -susceptible maize hybrids. *J. Agric. Food Chem*. **1999**, *47*, 299−304.
(18) Shukla, A.; Nycholat, C.; Mani, V. S.; Richard, J. A.; Malaolm, D. D. Use of resistant ACCase mutants to screen for novel inhibitors against resistant and susceptible forms of ACCase from grass weeds. *J. Agric. Food Chem.* **2004**, *52*, 5144−5150.

(19) Zhang, H.; Tweet, B.; Tong, L. Molecular basis for the inhibiton of the carboxyltransferase domain of acetyl coenzyme-A carboxylase by haloxyfop and diclofop. *Proc. Natl. Acad. Sci. U.S.A.* **2004**, *101*, 5910−5915.
(20) Zhao, H. J.; Wang, J. H.; Gao, P.; Zhang, J. Q.; Wang, T. Y.; Wang, G. Y. Cloning of plastid acetyl-CoA carboxylase cDNA from Setariaitlica and sequence analysis graminicide target site. *Acta Biontaica Sinica* **2004**, *46*, 751−756.
(21) National Center for Biotechnology Information. http://www.ncbi.nlm.nih.gov (accessed May 2005).
(22) Schwede, T.; Kopp, J.; Guex, N.; Peitsch, M. C. SWISS-MODEL: An automated protein homology-modeling server. *Nucleic Acids Res*. **2003**, *31*, 3381−3385.
(23) Zhang, H. L.; Benjiamin, T.; Jiang, L.; Liang, T. Crystal structure of the carboxyltransferase domain of acetyl-coenzyme A carboxylase in complex with CP-640186. *Structure* **2004**, *12*, 1683−1691.
(24) Laskowski, R. A.; MacArthur, M. W.; Moss, D. S.; Thornton, J. M. PROCHECK: A program to check the stereochemical quality of protein structures. *J. Appl. Crystallogr*. **1993**, *26*, 283−291.
(25) Rullmann, J. A. C. *AQUA*; Utrecht University: Utrecht, The Netherlands, 1996.
(26) Case, D. A.; Pearlman, D. A.; Caldwell, J. W.; Cheatham, T. E., III; Wang, J.; Ross, W. S.; Simmerling, C. L.; Darden, T. A.; Merz, K. M.; Stanton, R. V.; Cheng, A. L.; Vincent, J. J.; Crowley, M.; Tsui, V.; Gohlke, H.; Radmer, R. J.; Duan, Y.; Pitera, J.; Massova, I.; Seibel, G. L.; Singh, U. C.; Weiner, P. K.; Kollman, P. A. *AMBER 7*; University of California, San Francisco, CA, 2002.
(27) Jorgensen, W. L.; Chandrasekhar, J.; Madura, J.; Klein, M. L. Comparison of simple potential functions for simulating liquid water. *J. Chem. Phys*. **1983**, *79*, 926−935.
(28) Darden, T.; York, D. L. Pedersen, Particle mesh Ewald: An N log(N) method for Ewald sums in large sysytem. *J. Chem. Phys*. **1993**, *98*, 10089−10092.
(29) Ryckaert, J. P.; Ciccotti, G.; Berendsen, H. J. C. Numerical intergration of the Cartesian equations of motion of a system with constraints: Molecular synamics of *n*-alkanes. *J. Comput. Phys.* **1977**, *23*, 327−341.
(30) Berendsen, H. J. C.; Postma, J. P. M.; van Gunsteren, W. F.; DiNola, A.; Haak, J. R. Molecular dynamics with coupling to an external bath. *J. Comput. Phys.* **1984**, *81*, 3684−3690.
(31) Sippl, M. J. Boltzmann's principle, knowledge-based mean fields and protein folding. An approach to the computational determination of protein structures. *J. Comput.-Aided Mol. Des*. **1993**, *7*, 473−501.
(32) Zagnitko, O.; Jelenska, J.; Tevzadze, G.; Haselkon, R.; Gornicki, P. An isoleucine/leucine residue in the carboxyltransferase domain if acetyl-CoA carboxylase is critical for interaction with aryloxyphenoxypropionate and cyclohexanedione. *Proc. Natl. Acad. Sci. U.S.A.* **2001**, *98*, 6617−6622.
(33) Nikolskaya, T.; Zagnitko, O.; Tevzadze, G.; Haselkon, R.; Gornicki, P. Herbicide sensitivity determinant of wheat plastid acetyl-Coa carboxylase is located in a 400-amino acid fragment of the carboxyltransferase domain. *Proc. Natl. Acad. Sci. U.S.A.* **1999**, *96*, 14647−14651.
(34) Délye, C.; Zhang, X. Q.; Claire, C.; Michel, S.; Powles, S. B. An isoleucine residue within the carboxyltransferase domain of multidomain acetyl-CoA carboxylase is a major determinant of sensitivity to aryloxyphenoxypropionate but not to cyclohexanedione. *Plant Physiol*. **2003**, *132*, 1716−1723.
(35) Délye, C.; Michel, S. 'Universal' primers for PCR-sequenceing of grass chloroplastic acetyl-CoA carboxylase domains involved in resistance to herbicides. *Weed Res.* **2005**, *45*, 323−330.
(36) Herbert, D.; Pricel, J.; Alban, C.; Dehaye, L.; Job, J.; Pallett, K. E.; Harwood, J. L. Kinetic studies on two isoforms of acetyl-CoA carboxylase from maize leaves. *Biochem. J*. **1996**, *318*, 997−1006.
(37) Anna, M.; Angelo, M. F. Homology modeling studies on human galactose-1-phosphate uridylytransferase and on its galactosemia-related mutant Q188R provide an explanation of molecular effects of the mutation on homo- and heterodimers. *J. Med. Chem*. **2005**, *48*, 773−779.
(38) Mcfadden, J. J.; Frear, D. S.; Magasager, E. R. Aryl hydroxylation of diclofop by a cytochrom P450 dependent monoxygenase from wheat. *Pestic. Biochem. Physiol*. **1989**, *34*, 92−100.
(39) Donald, W. W.; Shimabukuro, R. H. Selectivity of diclofopmethyl between wheat and wild oat: Growth and herbicide metabolism. *Physiol. Plant* **1980**, *49*, 459−464.
(40) Steve, R. W.; Christopher Hall, J. Development and evaluation of an immumologocal approach for the identification of novel acetyl coenzyme-A carboxylase inhibitors: Assay optimization and pilot screen results. *J. Agric. Food. Chem.* **2000**, *48*, 1219−1228.
(41) James, A. T.; Daniel, J. P. Origin of enantiomeric selectivity in the aryloxyphenoxypropionic acid class of herbicidal acetyl coenzyme A carboxylase (ACCase) inhibitors. *J. Agric. Food. Chem*. **2002**, *50*, 4554−4566.

CI0600307